A density oscillator model

A. Hubard
Benjamin Levich Institute, City College of CUNY,
140th Street and Convent Avenue, New York, N.Y. 10031, USA.

C. Málaga, H. Arce, and H. González
Departamento de Física, Facultad de Ciencias, Universidad Nacional Auntónoma de México,
Mexico City 04510, D.F. Mexico.

Recibido el 12 de junio de 2012; aceptado el 9 de agosto de 2012

We present a model equation describing the behavior of a density oscillator and a set of experiments to test the model. The system consists of a cup containing salty water with an orifice in its base, partially submerged in an outer vessel filled with fresh water. Such a setup produces an oscillatory flow of water through the orifice. The density oscillator is an oscillatory system that shares common features with more complex systems with a stable limit cycle. Although a Rayleigh equation has been used as a model equation for these systems, we propose a different approach based on the integration of the hydrodynamic equations on a streamline. The model reproduces the experimental oscillation and predicts the period as a function of the physical parameters. Phase resetting curves observed in experiments under external biphasic excitation can be reproduced by the model.

Keywords: Density oscillator; saline oscillator; non-linear oscillators.

PACS: 47.20.Bp; 82.40.Bj

1. Introduction

There are plenty of systems in nature whose behavior resembles that of a non-linear oscillator with a limit cycle, such as electrochemical reactions [1], electromechanical devices [2], animal and plant populations, and physiological systems [3]. Non-linear oscillator models have been applied to locomotion [4], genetic networks [5] and biochemical reactions [6]. The application of periodic perturbations represents a way of studying and controlling such systems. In some cases, the effect of a single perturbation delivered at different phases is studied and summarized as the "Phase Transition Curve" (PTC) [7]. Heart-cell behavior has been characterized with this procedure [8].

The density oscillator is a relatively simple experimental device with an oscillatory behavior showing a stable limit cycle, a feature shared with many other non-linear oscillators. Its study will allow us to gain insight in the behavior and procedures applicable to more complex systems as cardiac and neural pacemakers and circadian rhythms [9]. The density oscillator is easy and inexpensive to build and has typically an oscillation period of tens of seconds that remains practically constant for hours, allowing easy manipulation.

This simple setup has been the subject of many studies, from the basic characterization of the oscillation [10,11] and its relation with the evolution of the electrical potential between the fresh and salty water or the inner and outer containers [12], to the coupled oscillation between two, three and many salty water cups in the same fresh water container [13-16]. Recently, the system behavior under single and periodic biphasic perturbations (pulses) has been reported, showing that the "Phase Transition Curve" can predict the phase-locking rhythms seen with periodic perturbations in experiments [9].

Nevertheless, existing models for the density oscillator behavior based on the Rayleigh equation [17] are not easily modified to include physical parameters describing perturbations. In this work we derive a model equation based on the Euler equations for an inviscid flow and compare its predictions for a perturbed density oscillator. First, the experimental setup is presented. The model derivation follows, results and comparisons are discussed at the end.

2. Experimental setup

The saline oscillator. The experimental set-up has been reported previously [9]. An inner container with an aqueous sodium chloride solution is partially immersed in an outer container containing fresh water (see Fig. 1). The outer container has 3.1 L of deionized water, with the water depth being 7.5 cm. The inner one contains 90 mL of 3M NaCl, with its bottom lying 4.1 cm above the bottom of the outer container. There is a pinhole in the center of the bottom of the inner container of 0.9 mm diameter and 2.2 mm depth. An acrylic plate with a hole in its center is placed across the top of the outer container to hold the inner container in place. A wooden plug, placed in the pinhole to prevent flow, is removed at the start of the experiment. The salty water initially flows downward through the pinhole, but after a few minutes the flow reverses, so that fresh water from the outer container flows upward through the pinhole. After several tens of seconds this upward flow stops, and the salty water begins to flow downward. This cycle repeats thousands of times over many hours until the oscillation stops. When there is flow, a voltage difference is generated between the two liquids [12,18,16,19]. This is recorded using two $Ag/AgCl_2$ electrodes, one placed in the salt water and the other placed in the fresh water.

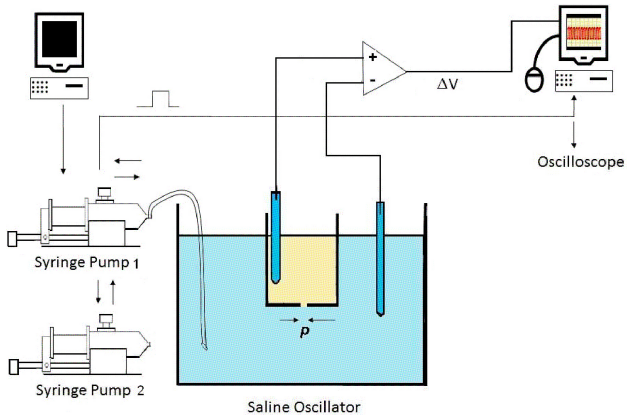

FIGURE 1. Experimental setup. Two pumps working in parallel are needed to infuse water swiftly.

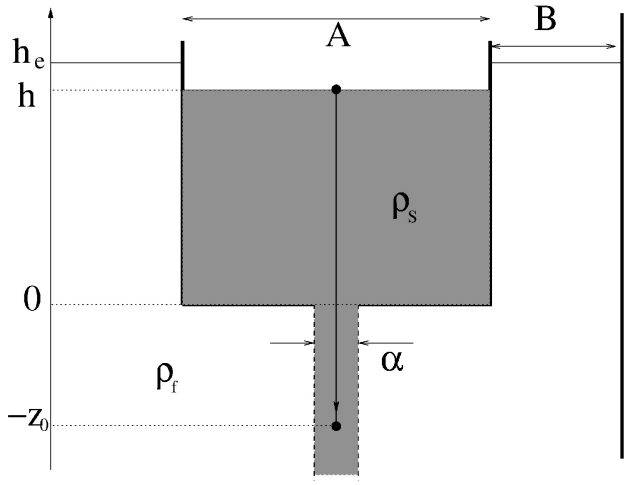

FIGURE 2. Diagram showing the line of integration when the salty water jet flows down inside the fresh water reservoir.

Volume pulse protocol. The oscillator is perturbed by infusing a fixed volume (1-4 mL) of fresh water into the bottom of the outer container and then withdrawing that same volume, using one or two syringe pumps driving two 60 mL syringes in parallel (WPI SP210iw Pump). This volume represents less than 0.15% of the total volume in the outer container. The flow rate in the pumps was adjusted by a computer-controlled interface so that the injection and withdrawal times are a small fraction of the natural period of the oscillation, 4% of $\sim$ 35 s (T_0). A biphasic pulse is used to prevent a long-lasting, cumulative effect on the volume - and thus the height - of the fluid.

Data recording and analysis. Both the voltage generated by the saline oscillator and a TTL signal that indicates when the pump was infusing were conditioned (InstruTech VR-10B; 47.2 kHz, 14-bit resolution) and recorded as a file with a PC data interface board (InstruTech VR-111, decimation factor of 128 leading to an effective sampling interval of 2.71 ms). The data was further decimated by a factor of 3 and passed through a Gaussian digital low-pass filter with $\sigma = 0.05$ [20]. To display, measure, and plot the data, we used Acquire-5.0.1, Review-5.0.1, and DataAccess-7.0.2 (Bruxton Corp.), as well as custom-written MATLAB programs.

Phase-resetting curve. As in our earlier study [9] we use the response of the oscillator to a single biphasic pulse, the phase-resetting response, to characterize the system behavior. The start of the cycle is taken to be the moment when the downwards flow of salty water initiates. In a phase-resetting run, a single biphasic volume pulse is delivered at a coupling time (T_c), defined as the time from the start of the cycle to the start of the pulse. The effect of this pulse is generally to change the duration of the cycle in which it is embedded (T_1). The duration of the following cycle, T_2, is typicaly unchanged from the control cycle length T_0. The phase at which the pulse is delivered is termed the old phase Φ, and is defined to be T_c/T_0, while the new phase Φ' is defined as $\Phi' = 1 - T_1/T_0 + T_c/T_0$ (modulo 1) [21]. The plot of Φ' vs. Φ is called the phase transition curve (PTC). Figure 6 shows PTCs obtained with different volumes. At each volume, three PTCs are shown, using data collected on three different days. For each PTC, there were ~ 50 pulses delivered. The oscillator was allowed to recover for five cycles between successive perturbations.

3. The Model

As has been done before [10-17], we will split the problem in two. We will separately study the fresh water jet ascending through salty water and the salty jet descending through fresh water. We will not attempt to describe what is happening during the time when a jet vanishes and the opposing jet develops.

Consider first the descending jet. We have fixed the origin of the coordinate system at the center of the inner vessel hole. If axial symmetry of the setup and flow is assumed, the axis of symmetry "z" passing through the center of the inner

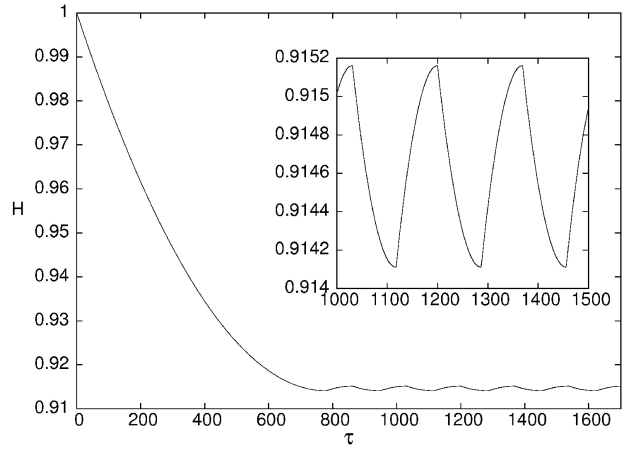

FIGURE 3. The evolution in time of the dimensionless salty water free surface height. The inset shows a close look at the height oscillation. Model parameters correspond to Yoshikawa *et al.* experiments [17].

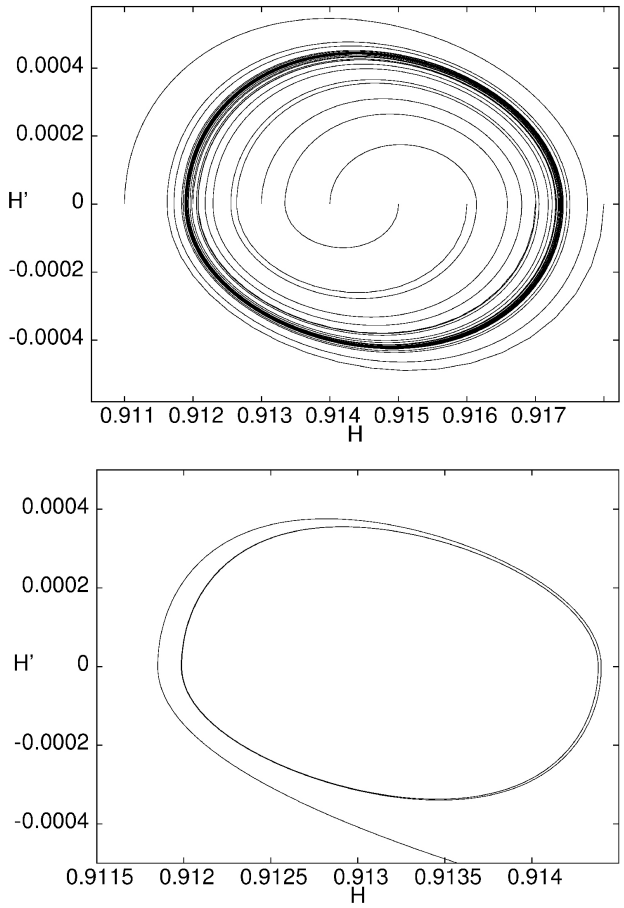

FIGURE 4. Top, a typical phase diagram of the movement of the dimensionless salty water free surface height for different initial conditions. Bottom, the phase diagram corresponding to Fig. 3, showing a fast convergence to the limit cycle.

vessel hole is a streamline (a curve tangent to the velocity field) and the velocity of the fluid elements on this axis will have only vertical component. This is a simplifying assumption that will provide an estimate of the pressure in the jet, the flow passing through the orifice and forming a jet may not be axis symmetrical.

One can integrate the Euler equations for the velocity $\mathbf{v}$ and the pressure p fields on an inviscid flow ($\rho(\partial\mathbf{v}/\partial\, t + \mathbf{v}\cdot\nabla\,\mathbf{v}) = -\nabla\, p + \rho\mathbf{g}$), projected along the axis of symmetry "z", from a point $-z_0$ below the inner vessel pinhole up to the salty water free surface h (see Fig. 2). This will provide a relation for the time evolution of the free surface $h(t)$ as long as it goes down.

$$\int_{-z_0}^{h}\left[\frac{\partial v_z}{\partial t}+\frac{\partial}{\partial z}\left(\frac{v_z^2}{2}\right)\right]dz = -\int_{-z_0}^{h}\frac{\partial}{\partial z}\left(\frac{p}{\rho_s}+gz\right)dz, \qquad (1)$$

where $v_z(z,t)$ and $p(z,t)$ are the vertical component of the velocity field and the pressure at the symmetry axis, g is the gravitational acceleration and ρ_s is the salty water density, since the line in the axis of symmetry remains inside the salty water region.

Although we have not measured the flow field, direct observation suggests an apparent unidirectional flow below a certain depth from the hole. Right below the hole, the jet must drag down the surrounding fresh water producing a local converging flow of fresh water outside the jet, but without contracting the jet as happens in the problem of the emptying tank, the "vena contracta" effect. Downstream, the jet has no apparent change in radius and there is no perceptible external flow except in the vertical direction. Flow incompressibility tells us that pressure inside and outside the jet at this depth will be a function of z only, but there could be a pressure jump when crossing radially the jet boundary, due to the abrupt change of density. If pressure outside the jet is z dependent and flow is neglegible as we move away from the jet radialy, then it may be approximated by its hydrostatic value.

Therefore, by integrating on a streamline starting somewhere below the hole ($-z_0$), in the center line of the jet, the pressure at that point can be estimated by the external hydrostatic pressure of fresh water at the same depth and its evolution in time. We take $p(-z_0) = p_{\text{atm}} + \rho_f g(h_e + z_0) - q(\rho_f - \rho_s)$, where the term $p_{\text{atm}} + \rho_f g(h_e + z_0)$ stands for the external hydrostatic pressure of fresh water of density ρ_f at a depth $h_e + z_0$, where h_e represents the level of the fresh water free surface, p_{atm} the atmospheric pressure and g the gravitational acceleration. The term $q(\rho_f - \rho_s)$ accounts for the pressure jump between points right inside and outside the jet, at the same depth, taken to be proportional, with constant q, to the density difference and considering that this difference will not change significantly during the period of time when the jet is fully developed. This appears to be the case as the interface that allows direct visual observation of the jet remains fixed and does not blur during the lifespan of the jet. Conservation of volume $V = Bh_e + Ah$ will, in turn, make this pressure proportional to h, as $h_e = (V - Ah)/B$, where A and B are, respectively, the areas of the salty and fresh water free surfaces. Hence

$$\int_{-z_0}^{h}\frac{\partial}{\partial z}\left(\frac{p}{\rho_s}+gz\right)dz = -\frac{\rho_f}{\rho_s}g\left(\frac{V-Ah}{B}+z_0\right) + q\left(\frac{\rho_f}{\rho_s}-1\right)+g(h+z_0). \qquad (2)$$

Notice that we are assuming that this all happens far from the bottom of the fresh water reservoir. Aside from the bottom region, fresh water movement far from the salty jet appears to be negligible if compared with the jet speed.

The integral of the inertial term $\partial v_z/\partial t$ in Eq. (1) can be estimated considering that a fluid element traveling down the streamline will accelerate from approximately h' to $h'A/\alpha$ inside the jet when crossing the pinhole, where h' is the speed of the salty water free surface and α stands for the area

of the pinhole. Hence the acceleration along the streamline will change from h'' above the hole to $h''A/\alpha$ inside the jet. This change happens over a distance that scales with $\sqrt{\alpha}$ and should represent the main contribution to the integral, this suggests that the inertial term scales as

$$\int_{-z_0}^{h} \frac{\partial v_z}{\partial t} dl \approx \frac{A}{\alpha} h''(z_0 + \sqrt{\alpha}). \tag{3}$$

We have neglected the contribution to the integral coming from $z = \sqrt{\alpha}$ to $z = h$ as it should scale with hh'', a much smaller contribution given that $A/\alpha \gg 1$ typically.

Finally, as the salty jet has roughly a fixed width, the velocity v_z at $z = -z_0$ is given by $h'A/\alpha$. Therefore, having scaled all terms in Eq. (1) by h and its derivatives, we arrive at a model equation for the descending salty jet given by

$$\frac{A}{\alpha} h'' \left(z_0 + \sqrt{\alpha}\right) + \frac{h'^2}{2} \left[1 - \left(\frac{A}{\alpha}\right)^2\right]$$
$$= \frac{\rho_f}{\rho_s} g \left(\frac{V - Ah}{B} + z_0\right) - q \left(\frac{\rho_f}{\rho_s} - 1\right) - g\left(h + z_0\right), \tag{4}$$

as long as $h' < 0$.

Similarly, for the ascending fresh jet the Euler equations are integrated on a streamline starting from a point l below the hole deep enough to consider the fluid at rest, up along the symmetry axis to a point z_0 above the hole, inside the jet. The same arguments lead to a similar equation for h when $h' > 0$ given by

$$\frac{A}{\alpha} h'' \left(z_0 + \sqrt{\alpha}\right) + \frac{h'^2}{2} \left(\frac{A}{\alpha}\right)^2 = \frac{\rho_s}{\rho_f} g \left(z_0 - h\right)$$
$$+ g \left(\frac{V - Ah}{B}\right) + q \left(\frac{\rho_s}{\rho_f} - 1\right) + g z_0. \tag{5}$$

To get dimensionless equations we scale distances with the characteristic height $h_0 = V/(A + B)$ (typically the initial inner and outer height) and time with $\sqrt{h_0/g}$ to arrive at two equations for the dimensionless height $H = h/h_0$ as a function of $\tau = t\sqrt{g/h_0}$,

$$L\ddot{H} = dc - H\left(1 + bd\right)$$
$$- Q\left(1 - d\right) + \epsilon\left(d - 1\right) - \frac{1}{2}\dot{H}^2\left(1 - a^2\right), \tag{6}$$

whenever $\dot{H} < 0$, and

$$L\ddot{H} = c - H\left(1 + \frac{1}{d}\right)$$
$$- Q\left(\frac{1}{d} - 1\right) + \epsilon\left(\frac{1}{d} - 1\right) - \frac{1}{2}\dot{H}^2 a^2, \tag{7}$$

whenever $\dot{H} > 0$.

The dimensionless parameters representing the setup geometry are $a = A/\alpha$, $b = A/B$ and $c = V/(Bh_0)$, and the density ratio $d = \rho_f/\rho_s$. These model equations have two free parameters given by the dimensionless distance from

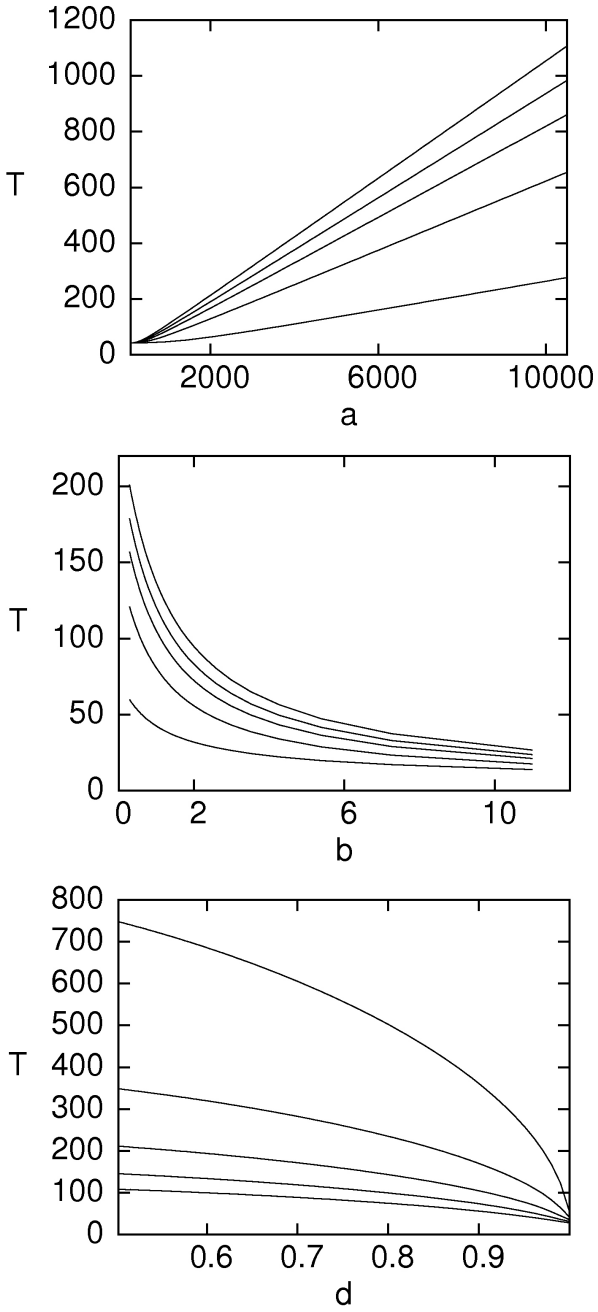

FIGURE 5. Dependence of the oscillating period on dimensionless parameters a, b and d, $\rho_f = 1$ for all curves. Top, the period as a function of the ratio of areas $a = A/\alpha$ for different values of ρ_s (1.01, 1.06, 1.11, 1.15 and 1.2), from $\rho_s = 1.01$, the lower curve, to $\rho_s = 1.2$, the upper curve. Middle, the period as a function of the ratio of areas $b = A/B$ for the same values of ρ_s, lower curve correspond to $\rho_s = 1.01$. Bottom, the period as a function of the density ratio $d = \rho_d/\rho_s$, for different values of a (418, 625, 1033, 2025 and 5625), from $a = 418$, the lower curve, to $a = 5625$, the upper curve.

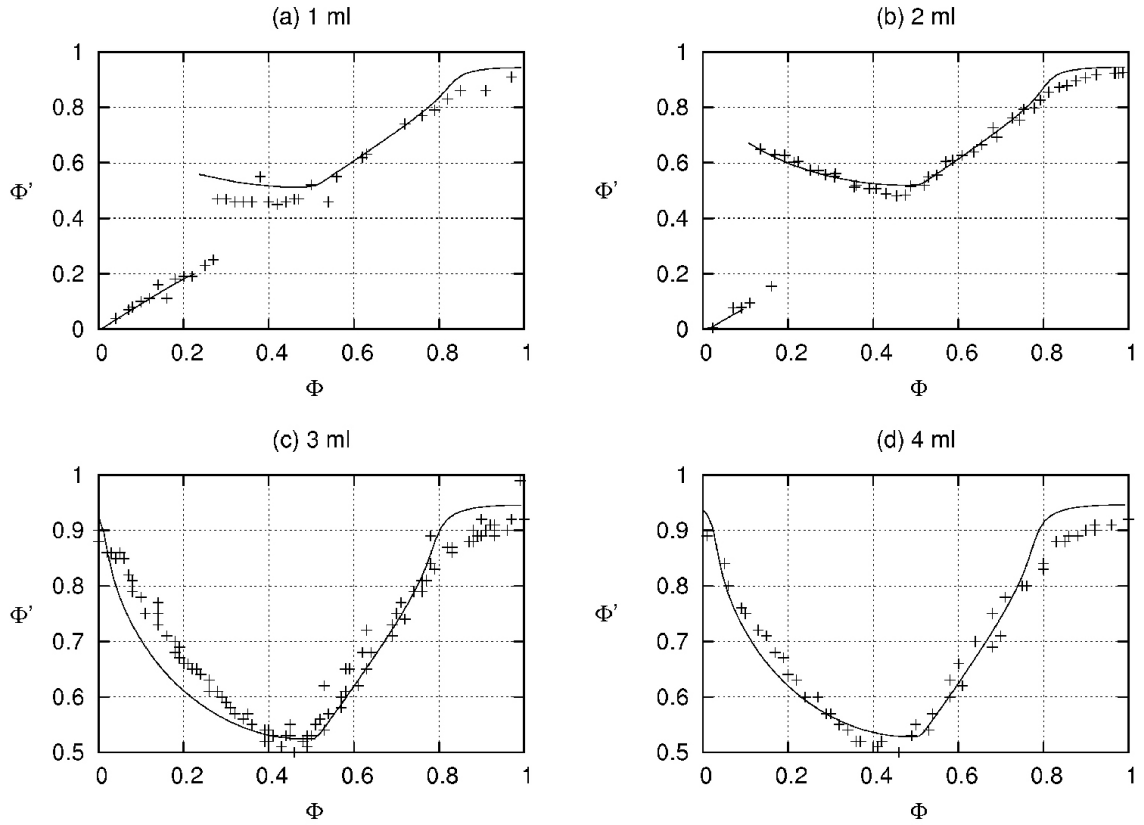

FIGURE 6. Comparison of the experimental PTC and the model predictions (continous line) for different pulse volumes.

the hole needed to have a unidirectional flow around the jet $\epsilon = z_0/h_0$ and the constant of proportionality between pressure and density gradients $Q = -q/(gh_0)$. The characteristic length of the inertial effects is given by $L = a(\epsilon + \sqrt{\alpha}/h_0)$.

Typically, experiments are performed starting with the free surface of the salty and fresh water at the same level, which produces a descending salty jet first. This corresponds to the initial conditions $H' = 0$ and a prescribed initial height H for the model Eq. (6). When H' changes sign, the ascending fresh water jet model Eq. (7) comes into play with initial conditions given by $H' = 0$ and the last value of H computed with Eq. (6). In this way, Eqs. (6) and (7) are alternated whenever H' changes sign to mimic the oscillation of the system.

Equations (6) and (7) have, respectively, an equilibrium points given by

$$H_{eq} = \frac{cd - Q(1-d) - \epsilon(1-d)}{1+db}, \tag{8}$$

and

$$H_{eq} = \frac{cd - Q(1-d) + \epsilon(1-d)}{1+db}. \tag{9}$$

Hence, the amplitude of oscillation is given roughly by the difference

$$\Delta H_{eq} = 2\frac{\epsilon(1-d)}{1+db}. \tag{10}$$

Therefore, the free parameter ϵ will allow us to adjust the amplitude of oscillation while the parameter Q will determine the height of the oscillation mid point relative to h_0.

Notice that the parameter c appears to be redundant as it is equal to $1 + b$ if volume V remains constant and the internal and external starting heights are equal. Nevertheless, in order to reproduce experiments in which the system is perturbed by including and removing small amounts of fresh water in the external reservoir, as the volume changes in time, the parameter $c = V(t)/(Bh_0)$ will be prescribed accordingly to account for these variations. Equations (6) and (7) remain unchanged if volume changes as its effect is still captured by the dependence of the hydrostatic fresh water pressure on V by c, only the characteristic height must be related to the initial volume corresponding to the unperturbed situation ($h_0 = V_0/(A + B)$).

Equations (6) and (7) can be integrated once to obtain

$$(\mathcal{H}')^2 = Ke^{-2\beta\mathcal{H}} - \tfrac{\gamma}{\beta}\left(\mathcal{H} - \tfrac{1}{2\beta}\right), \tag{11}$$

where the constant K is determined by the initial conditions and the various parameters and functions are defined as

$$\mathcal{H} = H - \frac{dc + (Q+\epsilon)(d-1)}{1+bd},$$

$$\gamma = \frac{1+bd}{L},$$

$$\beta = \frac{1-a^2}{2L},$$

when $H' < 0$, and

$$\mathcal{H} = H - \frac{dc + (Q-\epsilon)(d-1)}{1+bd},$$
$$\gamma = \frac{b+1/d}{L},$$
$$\beta = \frac{a^2}{2L},$$

when $H' > 0$.

These model equations for the oscillating height may be solved and compared to experiments by fitting the free parameters Q and ϵ. In the following section, the behavior of the model equation and its comparison with experiments is discussed.

4. Results

In order to model the density oscillator, Eqs. (6) and (7) are numerically integrated, alternating one after the other every time H' changes sign. A typical result is shown in Fig. 3 in which the model parameters have been chosen to reproduce the Okamura *et al.* experimental measurements of the height evolution [17]. Notice that, after an initial long discharge, oscillations occur around $h = 0.9146$, this is the equilibrium hydrostatic state, an unstable equilibria as the inital density distribution will not comply with hydrostatic conditions demanding a density profile vertically stratified. In this particular case, when the parameter ϵ was chosen to adjust the oscillation amplitude to that observed by Okamura *et al.*, the oscillating period predicted by the model was half the period reported in the experiments. Paradoxically, full Navier-Stokes simulations performed by Okamura *et al.* predicted twice the observed period. Okamura *et al.* argued that the oscillating period was sensitive to the shape of the orifice. In our case this could also be the reason, as viscous effects are not included and must be responsible for the sensitivity to the boundary conditions and a dampening effect that must lead to longer jet lifespans. As can be seen in Fig. 4, the behavior of the model in phase space resembles that of a limit cycle exhibited also by the Rayleigh equation. Additionally, the model suggests the behavior of the period of oscillation as a function of the physical parameters shown in Fig. 5. In particular, dependence on the area ratio a shows the same trend observed in the experiments by Alfredsson and Lagerstedt [22], the period increases as the orifice area decreases. The dependence of the period on b shows that it increases as the fresh water free surface is made bigger, as it takes more time for the salty jet to discharge enough mass and elevate the fresh water free surface and build enough hydrostatic pressure to stop the jet. Last figure shows that the period grows as the salty water gets denser, suggesting that a heavier salty water jet needs more pressure to stop.

In order to further test the model, we compared with experiments in which the oscillator is perturbed by adding and subtracting a small amount of fresh water in the external reservoir at different times during an oscillating period, *i.e.*, the phase reseting experiments previously described. Model parameters a, b, c and d were taken from the experimental setup, the free parameters Q and ϵ were taken from the fitting with Okamura's experiments [17], the only available data that follow the free surface height with time.

Figure 6 shows a comparison of the PTC behavior of the model against experimental data for different values of the fresh water added volume. To compare with the modelled results, the parameter c was increased by an amount δc during a lapse of time of 4% of the original modeled period (T_0), as in the experiments. Comparison with the experiments of added volumes of 1, 2, 3 and 4 ml was made with parameter values $\delta c = 0.0035, 0.007, 0.0105, 0.014$ respectively. This shows the model exhibits the right trend, which is not surprising as the volume dependence of Eqs. (7) and (6) comes from mass conservation, the least dubious of the assumptions made. These comparisons also show experimental PTC data reach a minimum at values of Φ barely below 0.5, while the model predicts a minimum at Φ a little bigger than 0.5. The reason of this discrepancy is the fact that the model predicts a descending jet that lasts longer than the ascending one, while experiments show the opposite behavior. It should be mentioned that the chosen values of δc to make comparison do not correspond to the experimentally added volumes, these values correspond to approximately three times those chosen and overestimate the PTC behavior.

5. Discussion

Notice that equations (6) and (7) are of the form

$$\ddot{H} = \lambda \dot{H}^2 + \omega H + I, \tag{12}$$

the coefficient λ is $(1/2)(a^2-1)/L \gg 1$ while $\dot{H} < 0$, and $(1/2)a^2/L \ll -1$ while $\dot{H} > 0$. Therefore the term $\lambda \dot{H}^2$ works as a damper as long as the right equation is chosen depending on the sign of $\dot{H}$. But the origin of this term is inertial, comes from the kinetic term in the Bernoulli equation. It must be noticed that neither of the model Eqs. (6) and (7) show an oscillatory behavior by themselves, it is the alternate use of them that mimics the oscillation. By themselves they do not include a dissipative mechanism that produce a limit cycle and Eq. (12) can not be regarded as a damped oscillator for a fixed value of λ.

Notice that the system can not stop until all salty water has left the inner cup and is replaced by fresh water, as hydrostatic conditions are always unstable while there is salty (heavier) water in the inner cup above fresh lighter water. The model suggests that jets originate as buoyancy driven instabilities and are stopped by the hydrostatic pressure building up around them. The system seems to oscillate between unstable equilibrium states.

The inhomogeneous forcing term I, equal to

$$\frac{1}{L}\left[dc-(Q+\epsilon)(1-d)\right] \text{ when } \dot{H}<0$$

and to

$$\frac{1}{dL}\left[dc-(Q-\epsilon)(1-d)\right] \text{ when } \dot{H}>0,$$

include the two fitting parameters Q and ϵ. Although they were included to model the pressure jump at the jet boundary and the distance from the orifice needed to observe a unidirectional flow around the jet, the role they play in the model equations is related to their unstable equilibrium point. Every time the equation is switched, the equilibrium point changes. For practical purposes, the free parameters Q and ϵ adjust the amplitude and midpoint of the oscillation. It must be acknowledge that it remains unclear to us how to relate them to their physical origins, specially ϵ that determines the end of the streamline, where the assumption of axial symmetry should give a good estimate of the pressure in the jet. A better understanding of the flow in the jet and its possible helical modes could provide a way of relating ϵ with the experimental parameters.

6. Conclusions

A system of model equations for the density oscillator based on the inviscid hydrodynamical equations was developed. The model predictions compare reasonably well with the observed behavior of the free surface evolution and PTC experiments. The model shows the same features that led previous investigators to use Rayleigh equations to model this system [17], which is basically having a limit cycle, with the benefit of a physical representation of the model parameters and a better adjustment to the PTC behavior and height oscillation behavior.

Acknowledgements

We want to thank Michel Guevara for his revision and valuable comments. Jaime García for his support with the experimental setup; Alicia Falcón and Araceli Torres for their help with data acquisition. This work was partially funded by PAPIIT-UNAM IN118611.

1. S. Nakata, K. Miyazaki, S. Izuhara, H. Yamaoka, and D. Tanaka, *J. Phys. Chem.* **113** (2009) 6876.
2. A. Ijspeert, J. Nakanishi and S. Schaal, *Learning rhythmic movements by demonstration using nonlinear oscillators*, in: (Proceedings of the 2002 IEEE/RSJ Intl. Conference on Intelligent Robots and Systems).
3. N. Loeuille and M. Ghil, *BMC Ecology* **4** (2004) 217.
4. A. Ijspeert, *Neural Networks* **21** (2008) 642.
5. J. Hallinan and J. Wiles, *Evolving genetic regulatory networks using an artificial genome.*, in: 2nd Asia-Pacfic Bioinformatics Conference (APBC2004).
6. M. Takinoue, *New Generation Computing* **27** (2009) 107.
7. M. R. Guevara and L. Glass, *J. Math. Biol.* **14** (1982) 1.
8. L. Glass, *Nonlinear Dynamics in Physiology and Medicine* (Springer- Verlag, New York, 2003) Chapter: Resetting and entraining biological rhythms.
9. H. González, H. Arce and M. R. Guevara, *Phys. Review E* **78** (2008) 036217.
10. S. Martin, *Geophysical Fluid Dynamics* (Gordon and Breach Science Publishers, 1970) Chapter: *A Hydrodynamic Curiosity: the Salt Oscillator*.
11. K. Yoshikawa, N. Oyama, M. Shoji and S. Nakata, *Am. J. Phys.* **59** (1991) 137.
12. K. Yoshikawa, S. Nakata, M. Yamanaka and T. Waki, *J. of Chemical Education* **66** (1989) 205.
13. S. Nakata, T. Miyata, N. Ojima and K. Yoshikawa, *Physica D* **115** (1998) 313.
14. K. Yoshikawa, K. Fukunaga, and M. Kawakami, *Chem. Phys. Lett.* **174** (1990) 203.
15. K. Miyakawa and K. Yamada, *Physica D* **151** (2001) 217.
16. K. Miyakawa and K. Yamada, *Physica D* **127** (1999) 177.
17. M. Okamura and K. Yoshikawa, *Phys. Review E* **61** (2000) 2445.
18. S. Upadhyay, A. K. Das, V. Agarwala and R. C. Srivastava, *Langmuir* **8** (1992) 2567.
19. R. P. Rastogi, R. C. Srivastava, and S. Kumar, *J. Colloid Interface Sci.* **283** (2005) 139.
20. J. Dempster, *Computer Analysis of Electrophysical Signals* (Academic Press, San Diego, 1993)
21. M. R. Guevara and A. Shrier, *Ann. N.Y. Acad. Sci.* **591** (1990) 11.
22. P. Alfredsson and T. Lagerstedt, *Physics of fluids* **24** (1981) 10.